analytical chemistry

Article

pubs.acs.org/ac

Fabrication of Sensitive Glutamate Biosensor Based on Vertically Aligned CNT Nanoelectrode Array and Investigating the Effect of CNTs density on the electrode performance

Azam Gholizadeh,[†] Saeed Shahrokhian,*[,†,‡] Azam Iraji zad,[†,§] Shamsoddin Mohajerzadeh,[∥] Manouchehr Vosoughi,[†,⊥] Sara Darbari,[∥] Javad Koohsorkhi,[∥] and Mahdiyeh Mehran[∥]

[†]Institute for Nanoscience and Nanotechnology (INST), Sharif University of Technology, Azadi Ave, Tehran, Iran

[‡]Department of Chemistry, Sharif University of Technology, Azadi Ave Tehran 11155-9516, Iran

[§]Department of Physics, Sharif University of Technology, Azadi Ave, Tehran, Iran

[∥]Thin Film and Nano-electronic Laboratory, Nano-electronic Center of Excellence, Department of Electrical and Computer Engineering, Faculty of Engineering, University of Tehran, North Karegar Ave., Tehran, Iran

[⊥]Chemical & Petroleum Engineering Department, Sharif University of Technology, Azadi Ave, Tehran, Iran

ABSTRACT: In this report, the fabrication of vertically aligned carbon nanotube nanoelectrode array (VACNT-NEA) by photolithography method is presented. Electrochemical impedance spectroscopy as well as cyclic voltammetry was performed to characterize the arrays with respect to different diffusion regimes. The fabricated array illustrated sigmoidal cyclic voltammogram with steady state current dominated by radial diffusion. The fabricated VACNT-NEA and high density VACNTs were employed as electrochemical glutamate biosensors. Glutamate dehydrogenase is covalently attached to the tip of CNTs. The voltammetric biosensor, based on high density VACNTs, exhibits a sensitivity of 0.976 mA mM^{-1} cm^{-2} in the range of 0.1−20 μM and 0.182 mA mM^{-1} cm^{-2} in the range of 20−300 μM glutamate with a low detection limit of 57 nM. Using the fabricated VACNT-NEA, the sensitivity increases approximately to a value of 2.2 Am M^{-1} cm^{-2} in the range of 0.01 to 20 μM and to 0.1 A mM^{-1} cm^{-2} in the range of 20−300 μM glutamate. Using this electrode, a record of low detection limit of 10 nM was achieved for glutamate. The results prove the efficacy of the fabricated NEA for low cost and highly sensitive enzymatic biosensor with high sensitivity well suited for voltammetric detection of a wide range of clinically important biomarkers.

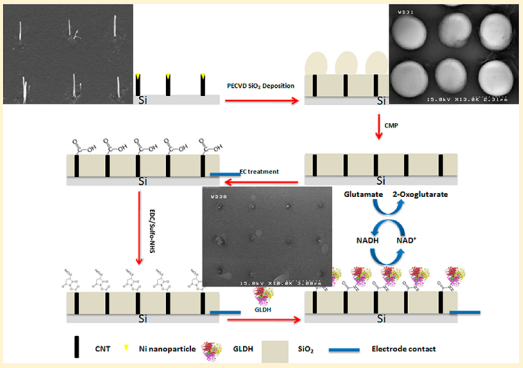

The transition from macrosize to microsize electrodes for electroanalytical applications began around three decades ago.[1,2] The main driving force behind this transition was the need for portable and in vivo sensing devices with an increased sensitivity, capable of measuring trace concentrations of analytes in ultrasmall sample volumes. The advantages of microelectrodes over macroelectrodes are largely attributed to the rapid formation of radial (three-dimensional) diffusion fields and reduced ohmic resistance effects, resulting in an increase in the mass transport rates, increased current densities and enhance signal-to-noise ratios.[3] These effects are assumed to be even more prominent in transition from micro- to nanosized electrodes.[4]

It is obvious that a single nanoelectrode generates a small current that is difficult to detect with conventional electrochemical setups. Fabricating arrays or ensembles of the nanoelectrodes amplify the measured current, which leads to a remarkable enhancement in the signal-to-noise ratio. For electrode arrays, in general, to benefit from these characteristics, the dimensions of the array need to fulfill certain requirements. To reach a regime where hemispherical diffusion layers of the neighboring electrodes do not overlap, the ratio of the interelectrode distance and the radius of a single electrode needs to be large enough depending on the time-scale of the experiment.[4−7] Therefore, the average interelectrode distance plays a crucial role in the fabrication of NEA. The fabrication of nanoelectrodes has been largely based on development methods used by the semiconductor industry using thin-film microfabrication technologies,[8] which have been widely used for the production of microelectronic chips and microelectromechanical systems (MEMS). The choice of the electrode material for the fabrication of NEA determines the overall sensing properties of the device. Carbon nanofibers and nanotubes, patterned using an E-beam lithography tool, have shown promising results for the realization of miniaturized NEA biosensors.[9−12] These entities possess both the advantages of ultra microelectrode arrays and unique electrochemical properties of CNT such as sensitivity improvement in

Received: February 16, 2012
Accepted: June 27, 2012
Published: June 27, 2012

   dx.doi.org/10.1021/ac300463x | *Anal. Chem.* 2012, 84, 5932−5938

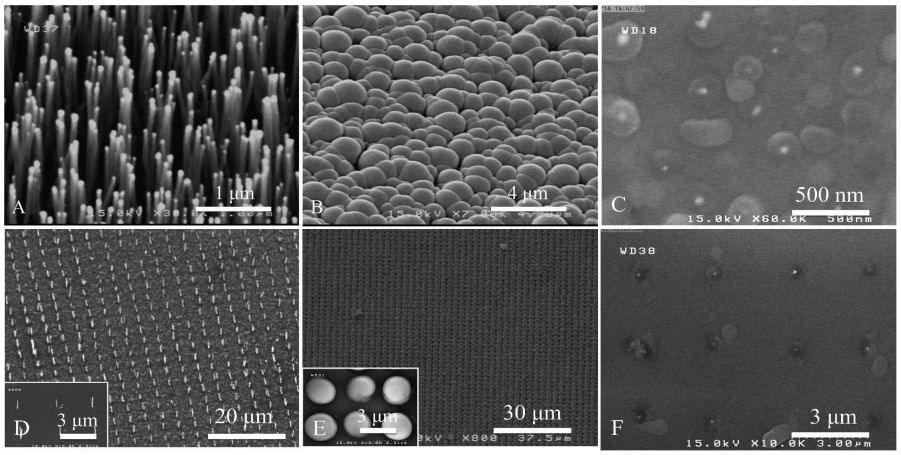

Figure 1. SEM images of (A) as-grown high density VACNTs, (B) the high density VACNTs embedded in SiO_2 matrix, (C) the surface of a polished high density VACNTs, (D) as-grown patterned array VACNTs using UV lithography, (E) the patterned VACNTs embedded in SiO_2 matrix, (F) the surface of a polished patterned VACNT array embedded in SiO_2 matrix. Images of A, B, D, and E are 45° perspective views, while images C, inset of E, and F are top views.

electrochemical biosensors. Because of the inherent electrocatalytic activity of these electrodes toward oxidation of H_2O_2 and NADH, and amplification of the electrochemical signals, these electrodes can be used as enzymatic biosensors. Especially, VACNTs are practically attractive since they can surmount the problems of CNT dispersion and transfer and offer a good attachment and electrical contact without using binders. They also prevent the degradation of enzymes on the electrode surface.

In the present work, a glutamate biosensor based on VACNT-NEA has been fabricated by means of photolithography combined with a reactive ion etching (RIE) technique as a postprocessing step to replace E-beam lithography. The performance of the fabricated biosensor has been compared to that of high-density VACNTs glutamate biosensors, presented by our group previously.[13] The effect of density of VACNTs was investigated on mediator-less voltammetric detection of glutamate, as an important amino acid which acts as an excitatory neurotransmitter in the central nervous system. The response of the electrochemical glutamate biosensors based on GLDH, used in this work, involves the oxidation of enzymatically generated nicotinamide adenine dinucleotide (NADH) given by eq 1.[14−16]

$$\text{Glutamate} + \text{NAD}^+ + \text{H}_2\text{O} \xrightarrow{\text{GLDH}} \text{2-oxoglutarate} + \text{NADH} + \text{NH}_4^+ + \text{H}^+ \quad (1)$$

The direct oxidation of NADH at unmodified electrodes requires large anodic over potentials owing to the slow kinetics of the electron transfer,[17] so various methodologies have been developed to facilitate the electron transfer kinetics for the oxidation of NADH. One of them is the application of CNTs in various forms.[18−23]

We have previously shown the mediator-less detection of glutamate at low over potential, only by covalently attaching GLDH to the VACNTs.[13] In this work, the performance of the biosensor significantly improved by using VACNT-NEA.

EXPERIMENTAL SECTION

Materials. Glutamic Dehydrogenase (GLDH, from bovine liver Type I as suspension in ammonium sulfate suspension, > 40 units/mg protein), L-Glutamic acid monosodium salt hydrate (>99%, TLC), and *N*-hydroxysulfosuccinimide sodium salt (sulfo-NHS) were purchased from Sigma/Aldrich. All other chemicals used in this investigation have analytical reagent grade provided by Merck. All solutions were prepared in deionized water (18.2 MΩ, Millipore Milli-Q system). Phosphate buffer solution (PBS, 0.1 M, pH 7.0) was employed as the supporting electrolyte in the electrochemical studies. Solutions of GLDH and NAD^+ were freshly prepared in the PBS of pH 7.0, immediately before each experiment.

Fabrication of VACNTs. Details of the fabrication of high density VACNTs are discussed in our previous report in reference 13. Concisely, the fabrication of NEA includes six steps: (1) A 8 nm thick nickel film is deposited using e-beam evaporation, and a 200 × 200 μm^2 square array with nickel dots with diameter of 700 nm and neighboring distance of 3 μm was patterned using high precision photolithography. (2) The diameter of the dots is reduced to 400 nm by means of a plasma ashing of the photoresist material in the reactive ion etching machine operated at 13.56 MHz and 150 W power in the presence of oxygen plasma with a pressure of 250 mTorr. (3) The growth of VACNTs was carried out using DC-PECVD. Prior to the growth process, a 15 min thermal annealing at a temperature of 650 °C and a hydrogenation step for 3 min were carried out. The VACNTs were grown in a mixture of C_2H_2/H_2 (5/18 sccm) at pressure of 1−5 Torr, temperature of 650 °C and power of 4 W cm^{-2}. (4) The CNTs were covered with a 2 μm SiO_2 layer by a RF-PECVD machine using a mixture of SiH_4/N_2 (8/200 sccm) and N_2O (200 sccm) at a temperature of 300 °C, pressure of 1 Torr, RF power of 40 W, and deposition rate of 50 nm min^{-1} to passivate the sidewalls of the nanotubes. (5) Since the tips of CNTs are also covered by oxide layer, a re-exposure step is needed to reach the buried tips. For this step, we used a chemical−mechanical polishing (CMP) as a planarization step. A 0.3 μm Al_2O_3 powder dissolved in 1 M KOH solution was used for rough polishing. The fine polish was carried out with 0.05 μm Al_2O_3 in 1 M KOH solution. During the chemical mechanical polishing process, CNT has been broken and probably a few nanometers of CNT walls are exposed from the SiO_2 layer. These tiny amounts of CNT walls should be removed before using the electrode. The excess wall of CNTs were removed by a 2 min

dx.doi.org/10.1021/ac300463x | *Anal. Chem.* 2012, 84, 5932−5938

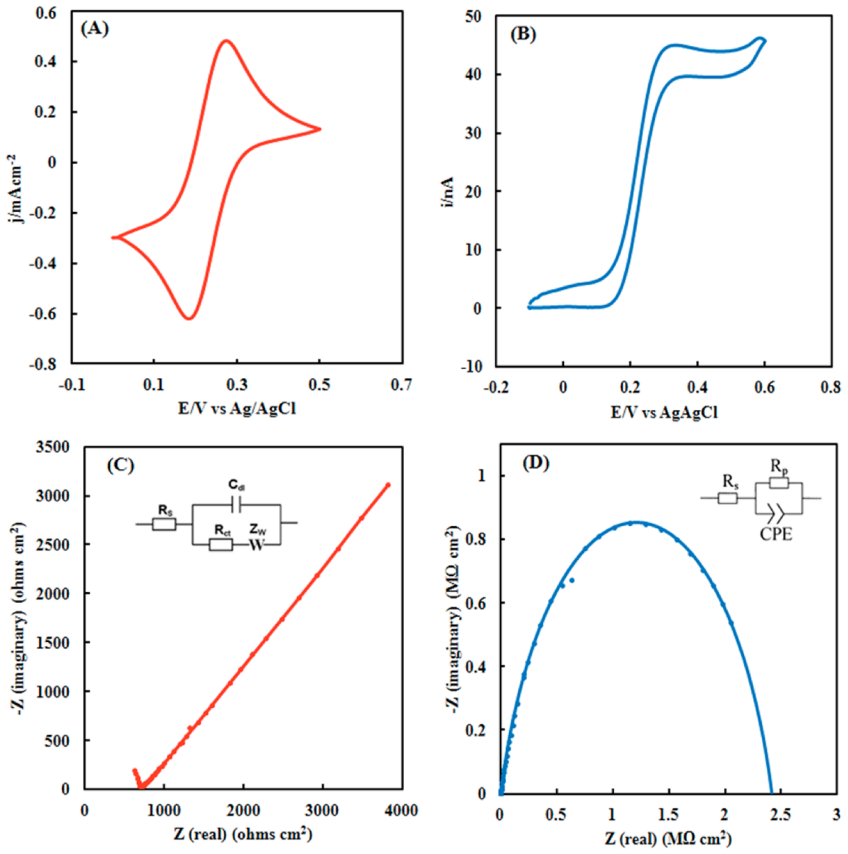

Figure 2. Cyclic voltammogram of (A) as-grown high density VACNTs after removing Ni nanoparticles, and (B) fabricated VACNT-NEA, Curve was taken in 5 mM $K_3Fe(CN)_6$ in a 0.1 M KCl at 20 mV s^{-1} scan rate. Electrochemical impedance spectrum of (C) as-grown high density VACNTs after removing Ni nanoparticles, and (D) fabricated VACNT-NEA, The spectrum was taken in 5 mM $K_4Fe(CN)_6$/5 mM $K_3Fe(CN)_6$, 0.1 M KCl in PBS (pH 7.4) at 0.1 Hz to 100 kHz and 0 V dc potential versus Ag/AgCl with ac potential amplitude of 10 mV.

ashing in Ar/O_2 plasma with RF power of 100 W. (6) A 10% HF solution was used to expose the contact layer.

Immobilization of the Enzyme on VACNTs. For both high density VACNTs and VACNT NEA after creation of carboxylic groups by electrochemical treatment in 1 M NaOH at 1.5 V for 30 s, GLDH was attached onto the end of the CNTs by using (1-(3-dimethylamino-propyl)-3-ethylcarbodiimide hydrochloride (EDC) and hydroxysulfo-succinimide sodium salt (sulfo-NHS) to promote amide linkages between the carboxyl-terminated nanotubes and the lysine residue of the protein. This was done by immersing the electrode in 1 mL freshly prepared PBS containing 10 mg mL^{-1} EDC and 30 mg mL^{-1} sulfo-NHS solution that was mixed carefully using a syringe needle and the reaction was allowed to occur at room temperature for 2 h. Then, after removing the excess solution of EDC and sulfo-NHS, 0.5 mL of enzyme (4 mg mL^{-1} in PBS) was placed on the electrode surface and the reaction was allowed to complete between the functionalized CNTs and the enzyme at room temperature for 2 h in the stirred solutions. Finally, the electrode was washed with a 0.1 M PBS of pH 7.4 containing 0.2% bovine serum albumin (BSA) and stored at 4 °C before use.

Electrochemical Measurements. Electrochemical experiments were performed with an IVIUM COMPACSTAT potentiostat/galvanostat in a three electrode setup using an O-ring Teflon cell consisting of VACNTs as the working electrode, together with an Ag/AgCl reference, and platinum counter electrodes. All voltammetric investigations were performed in deoxygenated solutions by purging with high purity nitrogen gas.

RESULTS AND DISCUSSION

Fabrication of VACNTs NEA. Forest VACNTs and VACNFs have a right size for NEA but they do not possess the right spacing, which needs to be at least 6 times larger than their radius. E-beam lithography has been used to control the density of such arrays,[9−12,24,25] But it is not a suitable candidate for commercial scale-up. In this work Ni film was patterned using ultraviolet photolithography followed by a plasma ashing process to reduce the size of the catalyst dots. Figures 1A and 1D show the grown VACNTs from a Ni film and arrays of nanoscale catalyst dots, respectively. To ensure obtaining a high value of signal-to-noise ratio with low background current, a defect free passivation layer is required. Also, the metal interconnects must not be in contact with the solution. Here, we used a radio frequency plasma-enhanced CVD (RF-PECVD) to grow the SiO_2 passivation layer. Figures 1B and 1E illustrate the embedded high and low density VACNTs in SiO_2 layer. The CMP was used for exposing the CNTs, because this process could remove any material independent of its type and density (SiO_2 around CNTs), and results in a smooth and highly planarized surface, resulting in exposed CNT tips.[26] Figures 1C and 1F illustrate the SiO_2 layer after planarization. Before application of the designed electrodes, their surfaces are exposed to oxygen plasma for a short time to ensure that the

dx.doi.org/10.1021/ac300463x | Anal. Chem. 2012, 84, 5932−5938

CNT walls are not short-circuited to the solution and the electron-transfer occurs only from the tips of the CNTs.

Electrochemical Characterization of VACNTs Density Effect Using CV and EIS. To be sure about the nanoelectrode behavior of low density VACNTs, their cyclic voltammetry (CV) curves must show a sigmoidal shape, which is an important characteristic of the steady-state mass transfer in a slow scan rate regime. For a disk electrode with 5 mm radius in an aqueous solution, the experimental time scale must be longer than 80 s. Therefore, steady state is not observed for macroelectrodes at the tens of mV s^{-1} time scale typical of conventional cyclic voltammetric experiments. However, reducing the electrode radius by a factor of 1 thousand to achieve a size of 5 μm, would cause the steady-state response to be observed in the time regimes longer than 80 μs. As the steady-state becomes more dominant with increasing time, the steady-state responses are easily observed for microelectrodes in the electrochemical experiments running at conventional time scales. So, if each of CNTs operates as a single nanoelectrode, the CV characteristic must change to sigmoidal shapes in conventional experiment time scales. Transition of diffusion regime from linear to radial is shown in Figure 2. Part A in this figure shows the CV curve of high density VACNTs at a scan rate of 20 mV s^{-1}, after opening the tips of the CNTs using Ni etchant. A quasi-reversible behavior (ΔE_p < 80 mV) can be proposed, to justify the increase of the peak potential separation (ΔE_p) with the scan rate. However, the fabricated VACNT-NEA shows a sigmoidal CV curve with the steady-state current dominated by radial diffusion (Figure 2B). The sigmoidal behavior of cyclic voltammetry shows that the electrode can be received steady state and there is no overlap of the diffusion layer from neighboring VACNT on the time scale of the experiment. Also the curves retain the same shape and i_{ss} remains the same with scan rate. The logarithm of the steady-state current plotted vs the logarithm of the scan rate, has a very small slope of <0.18.

AC impedance spectroscopy is considered as one of the best methods for characterizing an electrochemical system, by which both Faradic and non-Faradic processes can be readily studied. A combination of ac impedance spectroscopy and ultramicroelectrodes provides a powerful tool to probe diverse electrochemical systems. In the case of spherical mass transfer at high frequencies, the response is dominated by the charge transfer resistance and double layer capacitance. Consequently, a semicircle may be observed in the complex plane similar to the behavior of electrodes with normal dimensions. However, at low frequencies the spherical mass transfer causes formation of a depressed semicircle instead of linear behavior observed for linear semi-infinite diffusion. For very small electrodes (ultramicroelectrodes) the mass transfer impedance becomes negligible and the flux approaches a constant value. Also on Bode phase-angle graph, a maximum is observed at low frequencies. Figure 2C shows the EIS spectrum of high density VACNTs which is appeared as a straight line, indicating the linear diffusion-controlled behavior of the system. The EIS spectrum of fabricated VACNT-NEA shows only one semicircle expected for NEA (Figure 2D) which is simply modeled with Randles circuit. The model parameters for the two systems are collected in Table 1.

The CV and EIS data prove the efficacy of the photolithography-based process to realize suitable for VACNTNEA fabrication. In order to approve the biosensor applicability of the array, the performance of glutamate biosensor fabricated by high density VACNTs and VACNT NEA will be compared in the next section.

Table 1. Electrochemical Parameters of High Density VACNT and VACNT-NEA

CV parameters for HD-VACNTs	ΔE_p (mV)	effective area (cm^2)	E_c (V)	E_a (V)
after removing Ni nanoparticles	80	0.016	0.270	0.190
EIS parameters for HD-VACNTs	R_S (ohm)	R_{CT} (ohm)	C_{dl} (nF)	
after removing Ni nanoparticles	87.1	539.2	1.11	
EIS parameters for VACNT-NEA	R_S (ohm)	R_{CT} (M ohm)	CPE (nF)	n
VACNT-NEA	4646	2.07	3.5	0.803

Fabrication of Glutamate Biosensor Based on VACNT NEA. Figure 3 shows the schematic of different steps for immobilization of the enzyme on low density VACNTs. After planarization using CMP and subsequent treating with O_2 plasma to ensure the complete removal of the disrupted carbons which have been created during the CMP, GLDH enzyme are attached on the tips of low density nanotubes. Then, an electrochemical treatment was achieved to convert most of the oxides at the CNT tips to carboxyl (−COOH) groups. In the next step, GLDH was attached onto the end of the CNTs by using (1-(3-dimethylamino-propyl)-3-ethyl-carbodiimide hydrochloride (EDC) and hydroxysulfosuccinimide sodium salt (sulfo-NHS) to promote amide linkages between the carboxyl-terminated nanotubes and the lysine residues of the protein. Finally, the electrode was washed with 0.1 M PBS of pH of 7.4 containing 0.2% bovine serum albumin (BSA), and stored at 4 °C before use.

The activity of the enzymatic biosensors shows strong dependence on pH, as well as temperature and concentration of coenzyme. In order to investigate the effect of density of VACNTs on the biosensor performance, the same optimum condition was also used for high density VACNTs.[13]

The analytical performance of the glutamate biosensor was explored by using differential pulse voltammetry (DPV) method. Figure 4A and B display DPV results for various concentrations of glutamate (1−400 μM) solutions, without mediator, using high and VACNT NEA, respectively. The peak current, appeared between −0.10 to −0.056 V, depends on the glutamate concentration on high density VACNTs electrode. The corresponding peak on VACNT-NEA became sharper and shifted to −0.14 V. Figure 4C and D show the calibration curves on high density VACNTs and VACNT-NEA, respectively, indicating the presence of two linear ranges in each case. At low substrate levels, because of enhancement of diffusive effects at the electrode surface, even small changes in concentration can result in a significant change in the electrode response. Also, at low glutamate levels the local concentration at the electrode surface is rapidly depleted as GLDH converts substrate into product, resulting in high sensitivity of the electrode response. At higher glutamate concentrations, the enzyme is supplied with substrate for a longer period of time and the reaction proceeds over a larger time window. This together with possibility of fouling the electrode surface by the reaction products, results in a lower slope. Also it attains to the saturation level at higher concentration as expected for Michaelis−Menten type enzyme kinetics. We evaluated the reproducibility and stability of DPV signals from three

dx.doi.org/10.1021/ac300463x | Anal. Chem. 2012, 84, 5932−5938

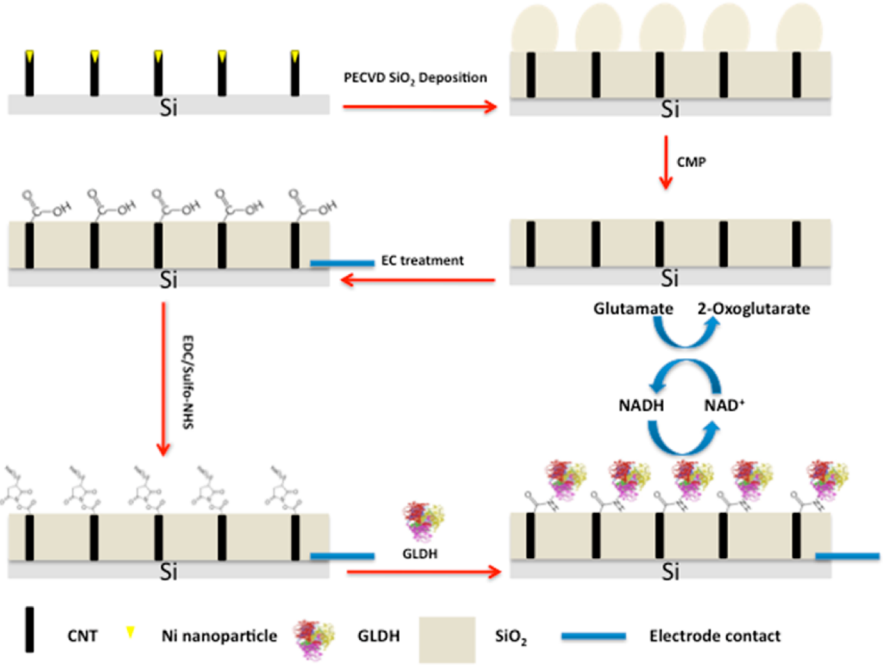

Figure 3. Schematic diagram illustrating the enzyme immobilization steps on VACNT-NEA.

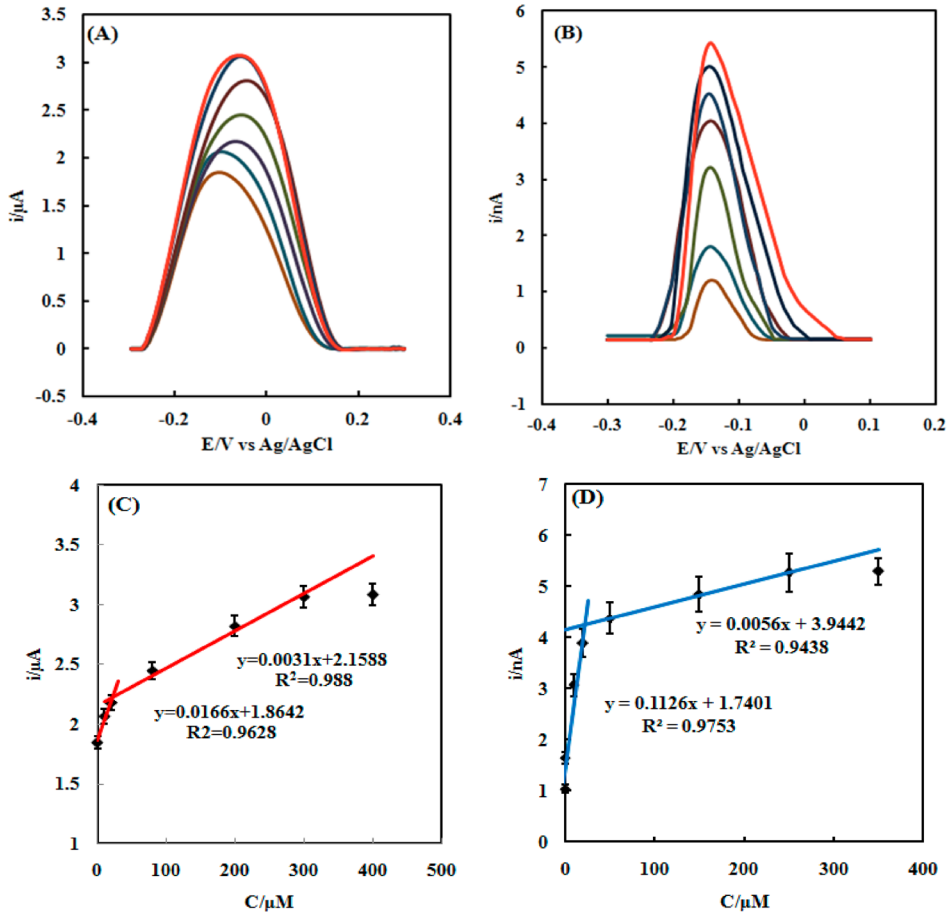

Figure 4. Differential pulse voltammograms of (A) different concentrations of glutamate (0.1, 1, 20, 80, 200, 300, and 400 μM) on high density VACNTs electrode, (B) different concentrations of glutamate (0.01, 0.1, 10, 20, 50, 150, and 250 μM) on VACNT-NEA. Calibration curves of (C) different concentrations of glutamate (0.1, 1, 20, 80, 200, 300, and 400 μM) on high density VACNTs electrode, (D) different concentrations of glutamate (0.01, 0.1, 10, 20, 50, 150, 250 and, 350 μM) VACNT-NEA. The curves were taken at the pulse amplitude of 50 mV, pulse width of 10 ms in PBS (0.1M, pH 7) containing 2 mM NAD^+.

dx.doi.org/10.1021/ac300463x | *Anal. Chem.* 2012, 84, 5932−5938

independent measurements that have been taken every 3 h so at least this electrode can be work for nine hours before regeneration.

To calculate the sensitivity for the high density VACNTs, the effective surface area of the electrode, calculated by Randles–Sevcik equation, was used. On the basis of the slope of the calibration curve, the biosensor based on high density VACNTs shows a sensitivity of 0.976 mA mM^{-1} cm^{-2} in the range of 0.1–20 μM and 0.182 mA mM^{-1} cm^{-2} in the range of 20–300 μM glutamate with a low detection limit of 57 nM. In calculation of the sensitivity for VACNT-NEA we suppose that each CNT acts as a ring which according to Ewing,[27] the limiting steady state current of a ring can be predicted from the current of a disk electrode with the same radius. Also it has been shown by Bard[28] that, for a ratio of inner radius/outer radius (a/b) of 0.2, the ring current is 99.8% of the disk. By refereeing to TEM images of CNTs,[29] this value seems to agree well for our electrode. So by simply assuming that each CNT resembles a disk, we can arrive at an estimate of the effective surface area of the electrode because the inner diameter of CNTs is much smaller than their wall thicknesses. Therefore, we can use the radial diffusion-limited steady-state current (i_{ss}) at the disk-like NEAs as *4NnFDCr* at 25 °C, where N is the number of exposed CNTs on the electrode, n is the number of electrons transferred per molecule, D (cm^2 s^{-1}) is the diffusion coefficient of the redox species, C (mol cm^{-3}) is the bulk concentration of the redox species, and r (cm) is the radius of the nanotubes. Based on the extracted values i_{ss}= 45 nA, D = 6.3 × 10^{-6} cm^2 s^{-1}, C = 5 mM, and r = 35 nm, n = 0.803 (obtained from EIS data), the effective number of nanotubes on the electrode surface is about 1340 and the effective surface area is approximately 5.15 × 10^{-8} cm^2. For VACNT-NEA based on the slope of the calibration curve, the biosensor has a sensitivity of 2.18 A mM^{-1} cm^{-2} in the range of 0.01–20 μM and 0.1 A mM^{-1} cm^{-2} in the range of 20–300 μM glutamate with a low detection limit of 10 nM.

CONCLUSION

In conclusion, VACNT-NEA were fabricated through a simple photolithography method combined with RIE technique, offers an inexpensive and simple alternative to E-beam lithography to obtain electrodes on area of around 200 × 200 μm^2. The surface of the electrode after each analysis can be refreshed by electrochemical treatment so the electrode can be used several times. The resulting array demonstrates sigmoidal voltammogram and impedance spectra which can be explained by spherical diffusion to the nanoelectrodes. The VACNT-NEA biosensor effectively responded to 0.01–300 μM glutamate with a current density of 2.18 A mM^{-1} cm^{-2} in the range of 0.01–20 μM and 0.1 A mM^{-1} cm^{-2} in the range of 20–300 μM. These promising results make the proposed electrode a suitable choice for detection of wide range of biomarkers. Also with rapid progress in science and realization of conservation, there is a high need for miniaturized analytical systems in various areas of modern life science, particularly with respect to micrototal analysis system (μTAS) or lab-on-a-chip (LOC) systems. The present NEA seems to be compatible with miniaturized analytical technology.

AUTHOR INFORMATION

Corresponding Author

*Tel.:+98-21-66005718. Fax: +98-21-66029165. E-mail: shahrokhian@sharif.edu.

Notes

The authors declare no competing financial interest.

ACKNOWLEDGMENTS

The authors gratefully acknowledge the support of this work by the Research Council and the Center of Excellence for Nanostructures of the Sharif University of Technology, Tehran, Iran. They are grateful to Professor Mohammad Kazem Amini (Department of Chemistry, University of Isfahan, Isfahan, Iran) for his valuable suggestions.

REFERENCES

(1) Zoski, C. G. *Electroanalysis* **2002**, *14*, 1041–1051.
(2) Dayton, M. A.; Brown, J. C.; Stutts, K. J.; Wightman, R. M. *Anal. Chem.* **1980**, *52*, 946–950.
(3) Berduque, A.; Lanyon, Y. H.; Beni, V.; Herzog, G.; Watson, Y.; Rodgers, E. K.; Stam, F.; Alderman, J.; Arrigan, D. W. M. *Talanta* **2007**, *71*, 1022–1030.
(4) Arrigan, D. W. M. *Analyst* **2004**, *129*, 1157–1165.
(5) Sandison, M. E.; Cooper, J. M. *Lab. Chip.* **2006**, *6*, 1020–1025.
(6) Gue, J.; Linder, E. *Anal. Chem.* **2009**, *81*, 130–138.
(7) Fleischmann, M.; Pons, S.; Daschbach, J. *J. Electroanal. Chem.* **1991**, *317*, 1–26.
(8) Sandison, M. E.; Anicet, N.; Glidle, A.; Cooper, J. M. *Anal. Chem.* **2002**, *74*, 5717–5725.
(9) Li, J.; Koehne, J.; Cassel, A. M.; Chen, H.; Ng, H.; Ye, Q.; Fan, W.; Han, J.; Meyyappan, M. *Inlaid Multi-Walled Carbon Nanotube Nanoelectrode Arrays for Electroanalysis*; Wiley-VCH: Verlag, Germany, 2005.
(10) Koehne, J.; Cassel, A. M.; Chen, H.; Ye, Q.; Ng, H.; Han, J.; Meyyappan, M. *J. Mater. Chem.* **2004**, *14*, 676–684.
(11) Tu, Y.; Lin, Y.; Yantasee, W.; Ren, Z. *Carbon Nanotube Based Nanoelectrode Arrays: Fabrication, Evaluation, and Application in Voltammetric Analysis*, Wiley-VCH: Verlag, Germany, 2005.
(12) Siddiqui, S.; Arumugam, P. U.; Chen, H.; Li, J.; Meyyappan, M. *ACS Nano* **2010**, *4*, 955–961.
(13) Gholizadeh, A.; Shahrokhian, S.; Iraji zad, A.; Mohajerzadeh, S.; Vosoughi, M.; Darbari, S.; Sanaee, Z. *Biosens. Bioelectron.* **2012**, *31*, 110–115.
(14) Olson Cosford, R. J.; Kuhr, W. G. *Anal. Chem.* **1996**, *68*, 2164–2169.
(15) Kuhr, W. G.; Barrett, V. L.; Gagnon, M. R.; Hopper, P.; Pantano, P. *Anal. Chem.* **1993**, *65*, 617–622.
(16) Pantano, P.; Kuhr, W. G. *Anal. Chem.* **1993**, *65*, 623–630.
(17) Moiroux, J.; Elving, P. J. *Anal. Chem.* **1978**, *50*, 1056–1062.
(18) Chakraborty, S.; Retna Raj, C. *Electrochem. Commun.* **2007**, *9*, 1323–1330.
(19) Tang, L.; Zhu, Y.; Yang, X.; Li, C. *Anal. Chim. Acta* **2007**, *597*, 145–149.
(20) Tang, L.; Zhu, Y.; Xu, L.; Yang, X.; Li, C. *Talanta* **2007**, *73*, 438–443.
(21) Rahman, M. M.; Umar, A.; Sawada, K. J. *Phys. Chem. B* **2009**, *113*, 1511–1516.
(22) Doaga, R.; McCormac, T.; Dempsey, E. *Electroanalysis* **2009**, *21*, 2099–2108.
(23) Meng, L.; Wu, P.; Chen, G.; Cai, C.; Sun, T.; Yuan, Z. *Biosens. Bioelectron.* **2009**, *24*, 1751–1756.
(24) Ren, Z. F.; Huang, Z. P.; Wang, D. Z.; Wen, J. G.; Xu, J. W.; Wang, J. H.; Cavet, L. E.; Chen, J.; Klemic, J. F.; Reed, M. A. *J. Appl. Phys. Lett.* **1999**, *75*, 1086–1088.
(25) Guillorn, M. A. T.; Melechko, E. A.; Merkulor, V. I.; Britt, P. F.; Austin, D. W.; Lowndes, D. H.; Simpson, M. L. *J. Appl. Phys.* **2002**, *91*, 3824–3828.
(26) Arumugam, P. U.; Chen, H.; Siddiqui, S.; Weinrich, J.; A. P.; Jejelowo, A.; Li, J.; Meyyappan, M. *Biosens. Bioelectron.* **2009**, *24*, 2818–2824.
(27) Wallingford, R. A.; Ewing, A. G. *Anal. Chem.* **1988**, *60*, 1972–1975.

(28) Lee, Y.; Amemiya, S.; Bard, A. J. *Anal. Chem.* **2001**, *73*, 2261−2267.
(29) Abdi, Y.; Mohajerzadeh, S.; Koohsorkhi, J.; Robertson, M. D.; Andrei, C. M. *Carbon* **2008**, *46*, 1611−1625.